mathematics

Article

Diffusion Simulation on Mammograms: A Technique for Analyzing and Monitoring Breast Tumors

Jonas Borjas [1], Kay Tucci [2], Orlando Alvarez-Llamoza [3,*] and Carlos Echeverria [1]

[1] CeSiMo, Facultad de Ingeniería, Universidad de Los Andes, Mérida 5101, Venezuela
[2] SUMA, Facultad de Ciencias, Universidad de Los Andes, Mérida 5101, Venezuela
[3] C^{2}MAD-CIITT, Universidad Católica de Cuenca, Cuenca 010101, Ecuador
* Correspondence: oalvarezll@ucacue.edu.ec

Abstract: We have developed an imaging biomarker for quantitatively monitoring the response to clinical treatment in cancer patients. Similar to other diffusion-weighted imaging DWI techniques, our method allows for the monitoring of breast cancer progression based on the diffusion coefficient values in the affected area. Our technique has the advantage of using images from mammograms and mesoscopic multiparticle collision MPC simulation, making it more affordable and easier to implement compared to other DWI techniques, such as diffusion-weighted MRI. To create our simulation, we start with the region of interest from a mammogram where the lesion is located and build a flat simulation box with impenetrable cylindrical obstacles of varying diameters to represent the tissue's heterogeneity. The volume of each obstacle is based on the intensity of the mammogram pixels, and the diffusion coefficient is calculated by simulating the behavior of a point particle fluid inside the box using MPC. We tested our technique on two mammograms of a male patient with a moderately differentiated breast ductal carcinoma lesion, taken before and after the first cycle of four chemotherapy sessions. As seen in other DWI studies, our technique demonstrated significant changes in the fluid concentration map of the tumor lesion, and the relative values of the diffusion coefficient showed a clear difference before and after chemotherapy.

Keywords: diffusion-weighted imaging; mesoscopic simulation; apparent diffusion coefficient; mammography image

MSC: 62H35; 68U20; 92C50

Citation: Borjas, J.; Tucci, K.; Alvarez-Llamoza, O.; Echeverria, C. Diffusion Simulation on Mammograms: A Technique for Analyzing and Monitoring Breast Tumors. *Mathematics* **2023**, *11*, 4988. https://doi.org/10.3390/math11244988

Academic Editor: Mariano Torrisi

Received: 29 November 2022
Revised: 11 January 2023
Accepted: 17 January 2023
Published: 18 December 2023

1. Introduction

Nowadays, many imaging methods are used to determine and diagnose breast lesions; some use diffusion-weighted magnetic resonance imaging techniques to map the diffusion of water molecules in tissues. These methods can detect and distinguish between malignant and benign breast lesions [1–4]. They have a notable ability to determine the density of tumor cells, their microstructure, and microvasculature at the cellular level without the use of contrast agents. One of them, the diffusion-weighted image (DWI) [5], coupled with morphological magnetic resonance imaging, improves the evaluation of treatment [6–8]. The DWI, combined with FDG–PET/CT (integrated positron emission tomography/computed tomography (PET/CT) with the glucose analog, 2-[(18)F]-fluoro-2-deoxy-d-glucose (FDG)), technique can predict the complete pathological response [9], and associated with dynamic contrast-enhanced magnetic resonance imaging, it can improve diagnosis [10–12]. DWI was also used to assess pathological response and surgical margins in locally advanced breast cancer patients [13], and the characterization of tumors is improved with high-resolution DWI [14,15].

An important parameter usually calculated using DWI is the apparent diffusion coefficient (ADC) [16]. It measures the diffusion of water in the tissue. The ADC reveals

some effects that the tissue produces on the diffusion coefficient of water, such as perfusion in capillary networks and incoherent intravoxel movement or non-Gaussian diffusion. This ability of ADC has attracted much interest from scientists and physicians in the last decade. Now, we know that the ADC values increase shortly after chemotherapy [17–20] and help to predict early response to these treatments [21–24]. Individualized ADC maps can help clinicians tailor treatments and avoid ineffective chemotherapies [25]. The ADC analysis, complemented with dynamic contrast magnetic resonance imaging, has also been used to determine tumor diameters [26]. The ADC difference has been shown to have the best predictive performance for the pathological response after neoadjuvant chemotherapy [27,28].

For breast lesions, mammography offers an alternative method to obtain images. The availability of equipment and the low cost for patients make mammograms a usual resource for analyzing and monitoring breast tumors. Unfortunately, obtaining diffusion-weighted images from mammograms to do an ADC analysis has not been possible. To solve this limitation, we propose to use a simulation method to calculate the diffusion coefficient using a mammogram. To do this, we convert the region of interest (ROI) taken from a mammogram into a simulation space where point fluid particles move through cylindrical obstacles representing the tissue's inhomogeneities [29]. The multiparticle collision (MPC) [30], a mesoscopic simulation technique, governs the dynamics of the particles. As the simulation space in MPC is continuous, the simulated fluid is affected even by small heterogeneities in the system. The effects of these variations are transmitted around the system by the hydrodynamic coupling. This behavior is essential to calculate average values, such as the mesoscopic diffusion coefficient (MDC). The outline of the paper is as follows. Section 2 describes the simulation technique, explains the mechanism for extracting the ROI from the mammogram, and constructs the simulation space. Next, in the same section, we present the simulation conditions, showing the parameters used to calculate the MDC. In Section 3, the results are presented. Finally, Section 4 contains the conclusions of this work.

2. MDC Calculation

The MPC technique has shown good hydrodynamic behavior in various homogeneous, heterogeneous, or crowded media, even to simulate binary fluids [31], catalytic chemical reactions [29,32,33], and protein dynamics [34–36]. Due to the coarse grain description, that is, the substitution of the collision calculation between particles by a rotational change in their velocities, the MPC technique is computationally efficient. It achieves all this by keeping the average momentum, energy, and mass constant in the system.

2.1. Building the Simulation Space from Mammograms

An application of diffusion coefficient measurement is monitoring a cancerous lesion treated with chemotherapy procedures. So, to present our method, we studied a 66-year-old male patient with a moderately differentiated ductal infiltrating neoplastic lesion before and after the first chemotherapy cycle. Figure 1 (top) shows the mammograms before (left) and after (right) the first cycle of four sessions with doxorubicin/endoxan according to the medical indications.

To extract the ROIs from the mammographic images, we use the image processing program ImageJ [37]. At the bottom of Figure 1, we observe the corresponding ROIs of each mammogram. In them, denser areas look lighter than less dense ones.

From the grayscale raster file of each ROI, we build a simulation box. The box's volume is given by $L_x \times L_y \times L_z$, where L_x and L_y are the numbers of rows and columns of the raster file, while the height is $L_z = 1$. We divide the simulation box into V small cubic cells of volume a^3, labeled by an index ξ. Each cell corresponds to a pixel of the raster image. Inside each of these cells, there is a cylindrical impenetrable obstacle reflecting tissue heterogeneity. Figure 2 shows a section of a simulation box corresponding to 4×3 pixels.

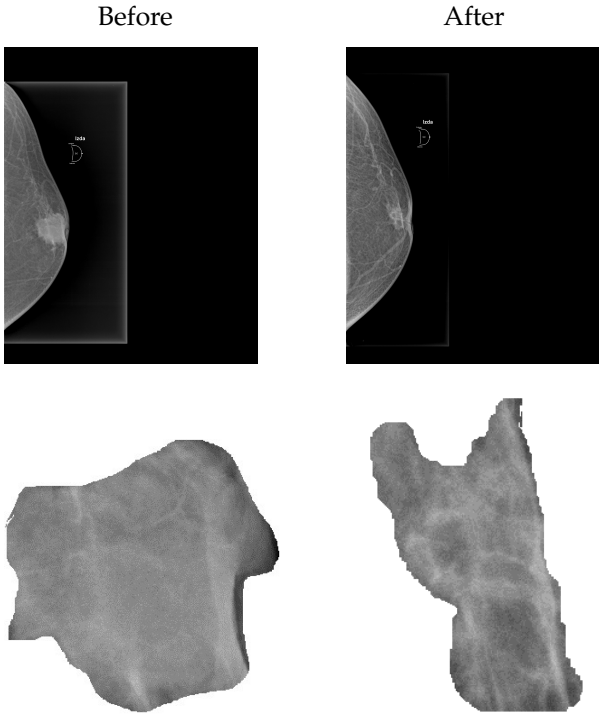

Figure 1. Mammograms of the patient before (left column) and after (right column) the first chemotherapy cycle. The original mammograms are on top. The respective ROIs extracted from the original mammograms using the image processing program ImageJ are on the bottom.

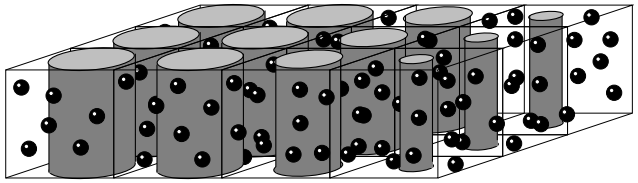

Figure 2. Section of a simulation box. The section corresponds to 4×3 pixels of the grayscale raster file of a ROI. The section dimension has $4 \times 3 \times 1$ cells. Inside each cell, there is a cylindrical obstacle. The cylinders with greater radii on the left represent darker pixels, i.e., areas with less dense tissue, and cylinders with smaller radii on the right correspond to lighter pixels, i.e., denser areas. The black spheres represent the point fluid particles.

The height of all cylinders is L_z while their radii are given by

$$r_\xi = \frac{1}{2}\left(1 - \frac{I_\xi}{2^b}\right), \qquad \text{with} \quad \xi = 1, 2, 3, \ldots, V\ ; \tag{1}$$

where r_ξ is the radius of the cylinder in the cell ξ, $I_\xi \in [0, 2^b]$ is the intensity of the ξ-th pixel of the raster file, and b is the color depth of the image.

Note that applying this method to an amorphous channel of cancerous cells, shown in mammograms as a lighter region, is mapped to a sequence of cells with cylinders with small radii ($r_\xi \approx 0$) or even without cylinders ($r_\xi = 0$). In the set of cells, particles move in a Brownian way. Instead, the darker regions that delimit these channels are represented by cells with cylinders with greater radii that can reach the maximum value of $r_\xi = L_z/2$.

This construction transfers the properties of the water movement inside a cancerous lesion to the simulated particles that move inside a rectangular plate of thickness L_z, crowded by cylinders of different radii.

2.2. Mesoscopic Technique

To start the MPC simulation, we put N identical particles of mass m into the simulation box, avoiding placing particles inside cylindrical obstacles. Additionally, each particle is assigned a random velocity according to a Maxwellian distribution [30]. Therefore, each particle has a given position and velocity $(\mathbf{x}_i, \mathbf{v}_i)$. In MPC dynamics, particles free stream between multiparticle collision events that occur at discrete times τ. We take obstacles as rigid and impenetrable cylindrical objects. When a particle collides with an obstacle, its velocity is reversed, and a bounce-back collision happens. These collisions can occur several times in the same interval τ. Multiparticle collisions carry out into the cells in the following way: At every time τ, a rotation operator $\hat{\omega}_\xi$, chosen randomly from some set of rotation operators, is assigned to each cell. After that, the post-collision velocity of particle i is given by:

$$\mathbf{v}_i' = \mathbf{V}_\xi + \hat{\omega}_\xi(\mathbf{v}_i - \mathbf{V}_\xi) \,, \tag{2}$$

where $\mathbf{V}_\xi$ is the center of mass velocity in the cell ξ given by

$$\mathbf{V}_\xi = n_\xi^{-1} \sum_{i=1}^{n_\xi} \mathbf{v}_i \,, \tag{3}$$

where n_ξ is the instantaneous number of particles in the cell ξ. Cells exchange momentum, mass, and energy with their neighbors. We set periodic boundary conditions in the simulation box to preserve the macroscopic properties of Newtonian fluids.

From previous studies with MPC simulations without obstacles, it is known that velocity correlations appear when the particles travel, on average, a small fraction of a cell side. To avoid this, we can introduce a random shift of the multiparticle collision grid to restore Galilean invariance [38]. However, our simulations use temperatures high enough to guarantee the invariance [31].

3. Results

A mean density of $n_0 = N/V = 10$ particles per cell was set to guarantee multiparticle collision events in all cells. The rotation operators $\hat{\omega}_\xi$ were taken from the set $\{\pm\pi/2\}$ about randomly chosen axes. The temperature in reduced units ($m = 1$, $a = 1$, $\tau = 1$) was $k_B T = 1$, where k_B is the Boltzmann constant. Thus, if $\bar{v} \sim (k_B T/m)^{1/2}$ is the average speed of the particles in the system, the mean free path, $\Lambda = \bar{v}\tau$, satisfies the relation $\Lambda/a \geqslant 1$ and ensures the conservation of the Galilean invariance.

Through simulation, we can observe the evolution of the density of particles in each cell of the system. The top of Figure 3 shows two snapshots of the initial fluid density and the bottom two snapshots of the density after $t = 500$ time steps.

The system images were built from the ROIs of mammograms taken before (left) and after (right) the chemotherapy. In the images, the intensity of the yellow color is proportional to the number of fluid particles present in each cell. Cells in red are those where the particle concentration is more than twice the initial value.

The final state of the simulations shows the regions where the fluid is highly concentrated. In these regions, the fluid, on average, has a longer residence time in cells due to its reduced mobility. In other words, the images bold the areas where the obstruction caused by the cancerous lesion is significant. Due to the hydrodynamic coupling, obstructions affect the entire system, decreasing the diffusion coefficient. Observe that the fluid density images offer the same information as DWI studies. Therefore, they can be used for the same purposes in evaluating and monitoring breast cancer.

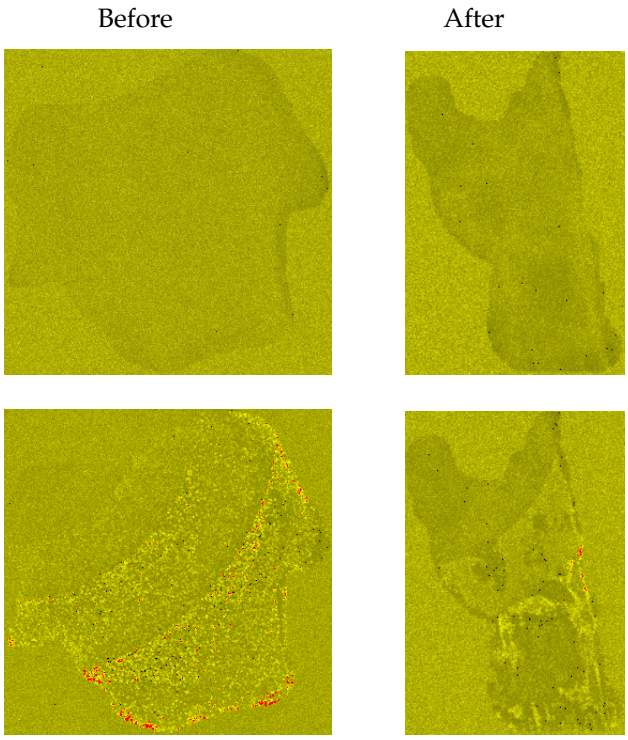

Figure 3. Snapshots of the simulated fluid density. The intensity of the yellow color is proportional to the fluid density. In red, the cells where the density exceeds twice the initial value. At left (right): images of the system built using the mammogram taken before (after) the first chemotherapy cycle. Top: $t = 0$. Bottom: $t = 500$ time steps.

We can calculate the mesoscopic diffusion coefficient through the Green-Kubo equation [39,40], given by:

$$MDC = \frac{1}{d}\int_0^\infty \langle \mathbf{v}_j(0) \cdot \mathbf{v}_j(t) \rangle dt \quad \text{with } j \in S\,, \tag{4}$$

where d is the dimension of the system, $\mathbf{v}_j(t)$ is the velocity of particle j at time t, and the angular brackets indicate an average over different initial conditions, starting times. Sets of labeled particles are S. To avoid the correlation effects on the z axis due to the thickness of the simulation box, $L_Z = 1$, we only use the x and y components of the velocities and set $d = 2$. We do the averages over three realizations and 50 stating time with 500 labeled particles.

To estimate how long the simulation is to obtain the value of MDC, we can observe the behavior of the velocity autocorrelation function, $C_\mathbf{v} = \langle \mathbf{v}_j(0) \cdot \mathbf{v}_j(t) \rangle$. Figure 4 shows a fast decay of $C_\mathbf{v}$ to values close to zero after $t = 5$ simulation steps.

To characterize the $C_\mathbf{v}$ decay, we adjust the points to the function $C_\mathbf{v} = \exp(-t/t_C)$ to obtain the characteristic times t_C. For the mammogram taken before the first chemotherapy cycle (circles), we have $\tau_C \approx 0.45$, and for the mammogram taken after (squares), we have $\tau_C \approx 0.58$. Therefore, we consider that $t = 100$ is enough time to estimate the value of MDC in Equation (4).

Remark that there are significant differences between the conditions in the tissue of the lesion and the simulation system in terms of spatial and temporal scale, speed or temperature, and amount of mass. Therefore, it is necessary to rescale both of them to compare the MCD with the diffusion coefficient in the actual tissue. The rescaled MDC is given by:

$$MDC^* = MDC/MDC_0\,, \tag{5}$$

where $MDC_0 = 1.167$ is the mesoscopic diffusion coefficient for a system without obstacles given by the theoretical relation [41]

$$MDC_0 = \frac{k_B T \tau}{2m} \left(\frac{2n_0 + 1 - e^{-n_0}}{n_0 - 1 + e^{-n_0}} \right) . \tag{6}$$

To compare our results, we have selected two previous studies, the first conducted by Hahn et al. [10] and the second by Partridge et al. [28]. Both measured the apparent diffusion coefficient (ADC) before and after the first chemotherapy cycle. In order to make the comparison, we also rescale ADC as follows:

$$ADC^* = ADC / ADC_H \, , \tag{7}$$

where ADC_H is the apparent diffusion coefficient of healthy tissues. Note that this rescaling reduces the dependency on the calibration of the measuring device [4]. As neither of these two studies reported the ADC_H values, we used the value $ADC_H = (1.78 \pm 0.13) \times 10^{-3}$ mm^2/s obtained in the third study by Sharma et al. [42].

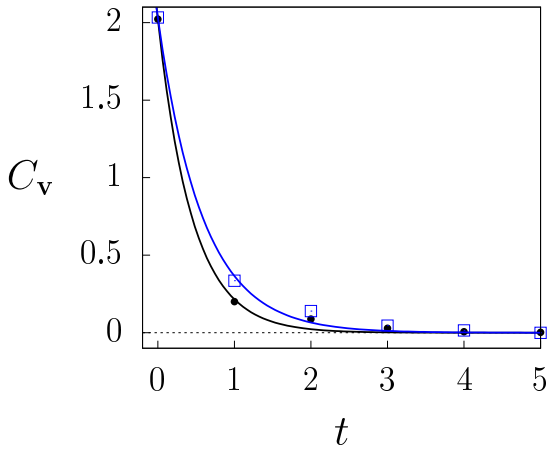

Figure 4. Evolution of the velocity autocorrelation function $C_{\mathbf{v}}$. The circles and squares represent the mammogram results before and after the first chemotherapy cycle. Solid lines are the best fit for equation $C_{\mathbf{v}} = \exp(-t/t_C)$. Points were obtained by averaging the realizations.

Table 1 compares the MDC^* before and after the first chemotherapy cycle obtained through simulation with the ADC^* values obtained through Equation (7).

Table 1. ADC^* and MDC^* values before and after the first chemotherapy cycle. Columns 2 and 3 show the ADC^* values obtained using the values of ADC reported by Partridge et al. [28] and Hahn et al. [10], respectively. At the bottom is the difference between the diffusion coefficients before and after the first chemotherapy cycle.

Study	***ADC****	***ADC****	***MDC****
Before	0.61 ± 0.06	0.52 ± 0.13	0.54 ± 0.03
After	0.70 ± 0.09	0.62 ± 0.24	0.63 ± 0.02
Δ_{DC}	0.09	0.10	0.09

Observe that there is a good agreement between the simulated values and those measured in these two previous works in both treatment stages, i.e., the results with ADC^* and MDC^* are statistically indistinguishable. Furthermore, the results obtained with MDC^* have minor errors and are statistically differentiated. A parameter to consider to measure the effectiveness of the applied treatment is the difference between the diffusion coefficients before and after the first chemotherapy cycle Δ_{DC} [28]. The value of Δ_{DC}

obtained using our technique is practically the same as those reported in the two previous studies conducted with DWI, as the bottom of Table 1 shows.

Usually, physicians can classify breast tumors as benign or malignant lesions. The ADC allows distinguishing between these two kinds of lesions. Table 2 shows the ADC^* obtained through the values reported by Yoshikawa et al. [43] and by Sharma et al. [42] for malignant and benign lesions.

Table 2. ADC^* values for malignant and benign breast lesions before any therapy.

Type	[42]	[43]
Malign	0.57 ± 0.06	0.55 ± 0.03
Benign	0.88 ± 0.08	0.72 ± 0.01

There is a good agreement between the values of ADC^* of malign lesions shown in Table 2 and the value of the mesoscopic diffusion coefficient before the chemotherapy cycle, $MDC^* = 0.54 \pm 0.03$, shown in Table 1. Moreover, even the value of the mesoscopic diffusion coefficient after the chemotherapy cycle, $MDC^* = 0.63 \pm 0.02$, is statistically different from the values of ADC^* of benign lesions.

Finally, all MPC simulations ran in a couple of hours on a 3400 GHz 7th generation I7 processor desktop computer, with a sequential algorithm executed on one of its cores. This performance shows that MPC dynamics can handle $N \approx 10^6$ fluid particles in a media with more than 65,000 obstacles in the heaviest calculation, all that on a standard personal computer.

4. Conclusions

We developed a technique that allows for the evaluation of cancerous lesions before and after a cycle of chemotherapy. The technique is based on the fact that cancerous lesions produce changes in tissue structure that alter the diffusion coefficient values in the affected area. Unlike other diffusion-weighted imaging (DWI) techniques that require specialized equipment such as magnetic resonators, our technique only requires a mammogram and a personal computer to simulate and calculate the diffusion coefficient.

We use multiparticle collision MPC dynamics to simulate fluid behavior inside tissues, which is a mesoscopic simulation technique that maintains the fundamental properties of fluids, such as hydrodynamic coupling and continuity in the diffusion space. MPC is efficient even when simulating fluids in crowded environments, making it well suited for our purpose.

The relative values obtained from the MPC simulations of the mesoscopic diffusion coefficient (MDC^*) are equivalent to the apparent diffusion coefficient (ADC^*) reported in previous studies of breast cancer lesions. Furthermore, our technique is able to measure a key parameter—the change in relative diffusion coefficient after the first cycle of chemotherapy (Δ_{DC})—that was found to be almost identical to that reported in previous studies conducted with other techniques. Additionally, our technique can differentiate malignant lesion and benign tumors.

The fact that our technique only requires a personal computer and mammograms makes it inexpensive and easy to implement and disseminate. Given these advantages, it is promising technique for the evaluation of cancerous lesion.

5. Patents

The methodology applied in this paper has been presented in the United States Patent and Trademark Office, with the title "Method for Monitoring and Analysis of Biomedical Images" under the provisional patent application number 2362.20100P.

Author Contributions: Conceptualization, C.E.; Methodology, C.E.; Software, K.T.; Validation, J.B.; Formal analysis, K.T. and C.E.; Investigation, O.A.-L.; Writing—original draft, K.T.; Writing—review & editing, O.A.-L. All authors have read and agreed to the published version of the manuscript.

Funding: The Jefatura de Investigación of the Universidad Católica de Cuenca, Ecuador, funded this article and its associated patent registration.

Data Availability Statement: Data available on request.

Acknowledgments: Kay Tucci and Carlos Echeverría thank ICTP for the fellowships from the PWF's programme Brain Gain Venezuela, whose goal is to fight brain drain by fostering the development of higher-level physics education and research carried out in Venezuela. Kay Tucci thanks Pacas foundation for the support through project MARCI114-K4FE and MC foundation through project G483R4-P014R.

Conflicts of Interest: The authors declare no conflict of interest.

References

1. Dorrius, M.D.; Dijkstra, H.; Oudkerk, M.; Sijens, P.E. Effect of b value and pre-admission of contrast on diagnostic accuracy of 1.5-T breast DWI: A systematic review and meta-analysis. *Eur. Radiol.* **2014**, *24*, 2835–2847. [CrossRef] [PubMed]
2. Shi, R.Y.; Yao, Q.Y.; Wu, L.M.; Xu, J.R. Breast lesions: Diagnosis using diffusion weighted imaging at 1.5 T and 3.0 T—Systematic review and meta-analysis. *Clin. Breast Cancer* **2018**, *18*, e305–e320. [CrossRef] [PubMed]
3. Chen, X.; Li, W.L.; Zhang, Y.L.; Wu, Q.; Guo, Y.M.; Bai, Z.L. Meta-analysis of quantitative diffusion-weighted MR imaging in the differential diagnosis of breast lesions. *BMC Cancer* **2010**, *10*, 693. [CrossRef] [PubMed]
4. Iima, M.; Honda, M.; Sigmund, E.E.; Ohno Kishimoto, A.; Kataoka, M.; Togashi, K. Diffusion MRI of the breast: Current status and future directions. *J. Magn. Reson. Imaging* **2019**, *52*, 70–90. [CrossRef] [PubMed]
5. Messina, C.; Bignone, R.; Bruno, A.; Bruno, A.; Bruno, F.; Calandri, M.; Caruso, D.; Coppolino, P.; De Robertis, R.; Gentili, F.; et al. Diffusion-weighted imaging in oncology: An update. *Cancers* **2020**, *12*, 1493. [CrossRef]
6. Belli, P.; Costantini, M.; Ierardi, C.; Bufi, E.; Amato, D.; Mule', A.; Nardone, L.; Terribile, D.; Bonomo, L. Diffusion-weighted imaging in evaluating the response to neoadjuvant breast cancer treatment. *Breast J.* **2011**, *17*, 610–619. [CrossRef] [PubMed]
7. Fangberget, A.; Nilsen, L.; Hole, K.H.; Holmen, M.; Engebraaten, O.; Naume, B.; Smith, H.J.; Olsen, D.R.; Seierstad, T. Neoadjuvant chemotherapy in breast cancer-response evaluation and prediction of response to treatment using dynamic contrast-enhanced and diffusion-weighted MR imaging. *Eur. Radiol.* **2011**, *21*, 1188–1199. [CrossRef]
8. Bufi, E.; Belli, P.; Di Matteo, M.; Terribile, D.; Franceschini, G.; Nardone, L.; Petrone, G.; Bonomo, L. Effect of breast cancer phenotype on diagnostic performance of MRI in the prediction to response to neoadjuvant treatment. *Eur. J. Radiol.* **2014**, *83*, 1631–1638. [CrossRef]
9. Park, S.H.; Moon, W.K.; Cho, N.; Chang, J.M.; Im, S.A.; Park, I.A.; Kang, K.W.; Han, W.; Noh, D.Y. Comparison of diffusion-weighted MR imaging and FDG PET/CT to predict pathological complete response to neoadjuvant chemotherapy in patients with breast cancer. *Eur. Radiol.* **2012**, *22*, 18–25. [CrossRef]
10. Hahn, S.Y.; Ko, E.Y.; Han, B.K.; Shin, J.H.; Ko, E.S. Role of diffusion-weighted imaging as an adjunct to contrast-enhanced breast MRI in evaluating residual breast cancer following neoadjuvant chemotherapy. *Eur. J. Radiol.* **2014**, *83*, 283–288. [CrossRef]
11. Li, X.; Abramson, R.G.; Arlinghaus, L.R.; Kang, H.; Chakravarthy, A.B.; Abramson, V.G.; Farley, J.; Mayer, I.A.; Kelley, M.C.; Meszoely, I.M.; et al. Multiparametric magnetic resonance imaging for predicting pathological response after the first cycle of neoadjuvant chemotherapy in breast cancer. *Investig. Radiol.* **2015**, *50*, 195–204. [CrossRef] [PubMed]
12. Minarikova, L.; Bogner, W.; Pinker, K.; Valkovič, L.; Zaric, O.; Bago-Horvath, Z.; Bartsch, R.; Helbich, T.H.; Trattnig, S.; Gruber, S. Investigating the prediction value of multiparametric magnetic resonance imaging at 3 T in response to neoadjuvant chemotherapy in breast cancer. *Eur. Radiol.* **2017**, *27*, 1901–1911. [CrossRef] [PubMed]
13. Agarwal, K.; Sharma, U.; Sah, R.G.; Mathur, S.; Hari, S.; Seenu, V.; Parshad, R.; Jagannathan, N.R. Pre-operative assessment of residual disease in locally advanced breast cancer patients: A sequential study by quantitative diffusion weighted MRI as a function of therapy. *Magn. Reson. Imaging* **2017**, *42*, 88–94. [CrossRef] [PubMed]
14. Wilmes, L.J.; McLaughlin, R.L.; Newitt, D.C.; Singer, L.; Sinha, S.P.; Proctor, E.; Wisner, D.J.; Saritas, E.U.; Kornak, J.; Shankaranarayanan, A.; et al. High-resolution diffusion-weighted imaging for monitoring breast cancer treatment response. *Acad. Radiol.* **2013**, *20*, 581–589. [CrossRef] [PubMed]
15. McLaughlin, R.L.; Newitt, D.C.; Wilmes, L.J.; Jones, E.F.; Wisner, D.J.; Kornak, J.; Proctor, E.; Joe, B.N.; Hylton, N.M. High resolution in vivo characterization of apparent diffusion coefficient at the tumor–stromal boundary of breast carcinomas: A pilot study to assess treatment response using proximity-dependent diffusion-weighted imaging. *J. Magn. Reson. Imaging* **2014**, *39*, 1308–1313. [CrossRef] [PubMed]
16. Hamstra, D.A.; Rehemtulla, A.; Ross, B.D. Diffusion magnetic resonance imaging: A biomarker for treatment response in oncology. *J. Clin. Oncol.* **2007**, *25*, 4104–4109. [CrossRef] [PubMed]

17. Li, X.R.; Cheng, L.Q.; Liu, M.; Zhang, Y.J.; Wang, J.D.; Zhang, A.L.; Song, X.; Li, J.; Zheng, Y.Q.; Liu, L. DW-MRI ADC values can predict treatment response in patients with locally advanced breast cancer undergoing neoadjuvant chemotherapy. *Med. Oncol.* **2012**, *29*, 425–431. [CrossRef]
18. Richard, R.; Thomassin, I.; Chapellier, M.; Scemama, A.; de Cremoux, P.; Varna, M.; Giacchetti, S.; Espié, M.; de Kerviler, E.; de Bazelaire, C. Diffusion-weighted MRI in pretreatment prediction of response to neoadjuvant chemotherapy in patients with breast cancer. *Eur. Radiol.* **2013**, *23*, 2420–2431. [CrossRef]
19. Iwasa, H.; Kubota, K.; Hamada, N.; Nogami, M.; Nishioka, A. Early prediction of response to neoadjuvant chemotherapy in patients with breast cancer using diffusion-weighted imaging and gray-scale ultrasonography. *Oncol. Rep.* **2014**, *31*, 1555–1560. [CrossRef]
20. Yuan, L.; Li, J.J.; Li, C.Q.; Yan, C.G.; Cheng, Z.L.; Wu, Y.K.; Hao, P.; Lin, B.Q.; Xu, Y.K. Diffusion-weighted MR imaging of locally advanced breast carcinoma: The optimal time window of predicting the early response to neoadjuvant chemotherapy. *Cancer Imaging* **2018**, *18*, 38. [CrossRef]
21. Sharma, U.; Danishad, K.K.A.; Seenu, V.; Jagannathan, N.R. Longitudinal study of the assessment by MRI and diffusion-weighted imaging of tumor response in patients with locally advanced breast cancer undergoing neoadjuvant chemotherapy. *NMR Biomed. Int. J. Devoted Dev. Appl. Magn. Reson. In Vivo* **2009**, *22*, 104–113. [CrossRef] [PubMed]
22. Shin, H.J.; Baek, H.M.; Ahn, J.H.; Baek, S.; Kim, H.; Cha, J.H.; Kim, H.H. Prediction of pathologic response to neoadjuvant chemotherapy in patients with breast cancer using diffusion-weighted imaging and MRS. *NMR Biomed.* **2012**, *25*, 1349–1359. [CrossRef] [PubMed]
23. Fujimoto, H.; Kazama, T.; Nagashima, T.; Sakakibara, M.; Suzuki, T.H.; Okubo, Y.; Shiina, N.; Fujisaki, K.; Ota, S.; Miyazaki, M. Diffusion-weighted imaging reflects pathological therapeutic response and relapse in breast cancer. *Breast Cancer* **2014**, *21*, 724–731. [CrossRef] [PubMed]
24. Liu, S.; Ren, R.; Chen, Z.; Wang, Y.; Fan, T.; Li, C.; Zhang, P. Diffusion-weighted imaging in assessing pathological response of tumor in breast cancer subtype to neoadjuvant chemotherapy. *J. Magn. Reson. Imaging* **2015**, *42*, 779–787. [CrossRef] [PubMed]
25. Park, S.H.; Moon, W.K.; Cho, N.; Song, I.C.; Chang, J.M.; Park, I.A.; Han, W.; Noh, D.Y. Diffusion-weighted MR imaging: Pretreatment prediction of response to neoadjuvant chemotherapy in patients with breast cancer. *Radiology* **2010**, *257*, 56–63. [CrossRef]
26. Jensen, L.R.; Garzon, B.; Heldahl, M.G.; Bathen, T.F.; Lundgren, S.; Gribbestad, I.S. Diffusion-weighted and dynamic contrast-enhanced MRI in evaluation of early treatment effects during neoadjuvant chemotherapy in breast cancer patients. *J. Magn. Reson. Imaging* **2011**, *34*, 1099–1109. [CrossRef]
27. Che, S.; Zhao, X.; Yanghan, O.; Li, J.; Wang, M.; Wu, B.; Zhou, C. Role of the intravoxel incoherent motion diffusion weighted imaging in the pre-treatment prediction and early response monitoring to neoadjuvant chemotherapy in locally advanced breast cancer. *Medicine* **2016**, *95*, e2420. [CrossRef]
28. Partridge, S.C.; Zhang, Z.; Newitt, D.C.; Gibbs, J.E.; Chenevert, T.L.; Rosen, M.A.; Bolan, P.J.; Marques, H.S.; Romanoff, J.; Cimino, L.; et al. Diffusion-weighted MRI findings predict pathologic response in neoadjuvant treatment of breast cancer: The ACRIN 6698 Multicenter Trial. *Radiology* **2018**, *289*, 618–627. [CrossRef]
29. Echeverria, C.; Kapral, R. Autocatalytic reaction dynamics in systems crowded by catalytic obstacles. *Phys. D Nonlinear Phenom.* **2010**, *239*, 791–796. [CrossRef]
30. Malevanets, A.; Kapral, R. Mesoscopic model for solvent dynamics. *J. Chem. Phys.* **1999**, *110*, 8605–8613. [CrossRef]
31. Echeverria, C.; Tucci, K.; Alvarez-Llamoza, O.; Orozco-Guillén, E.; Morales, M.; Cosenza, M. Mesoscopic model for binary fluids. *Front. Phys.* **2017**, *12*, 128703. [CrossRef]
32. Echeveria, C.; Tucci, K.; Kapral, R. Diffusion and reaction in crowded environments. *J. Phys. Condens. Matter* **2007**, *19*, 065146. [CrossRef]
33. Echeverria, C.; Herrera, J.L.; Alvarez-Llamoza, O.; Morales, M.; Tucci, K. Damping and clustering into crowded environment of catalytic chemical oscillators. *Phys. A Stat. Mech. Its Appl.* **2019**, *517*, 297–306. [CrossRef]
34. Echeverria, C.; Kapral, R. Macromolecular dynamics in crowded environments. *J. Chem. Phys.* **2010**, *132*, 104902. [CrossRef] [PubMed]
35. Echeverria, C.; Kapral, R. Molecular crowding and protein enzymatic dynamics. *Phys. Chem. Chem. Phys.* **2012**, *14*, 6755–6763. [CrossRef] [PubMed]
36. Echeverria, C.; Kapral, R. Enzyme kinetics and transport in a system crowded by mobile macromolecules. *Phys. Chem. Chem. Phys.* **2015**, *17*, 29243–29250. [CrossRef] [PubMed]
37. Collins, T.J. ImageJ for microscopy. *Biotechniques* **2007**, *43*, S25–S30. [CrossRef]
38. Ihle, T.; Kroll, D. Stochastic rotation dynamics: A Galilean-invariant mesoscopic model for fluid flow. *Phys. Rev. E* **2001**, *63*, 020201. [CrossRef]
39. Green, M.S. Markoff random processes and the statistical mechanics of time-dependent phenomena. II. Irreversible processes in fluids. *J. Chem. Phys.* **1954**, *22*, 398–413. [CrossRef]
40. Kubo, R. Statistical-mechanical theory of irreversible processes. I. General theory and simple applications to magnetic and conduction problems. *J. Phys. Soc. Jpn.* **1957**, *12*, 570–586. [CrossRef]
41. Kapral, R. Multiparticle collision dynamics: Simulation of complex systems on mesoscales. *Adv. Chem. Phys.* **2008**, *140*, 89.

42. Sharma, U.; Sah, R.G.; Agarwal, K.; Parshad, R.; Seenu, V.; Mathur, S.R.; Hari, S.; Jagannathan, N.R. Potential of diffusion-weighted imaging in the characterization of malignant, benign, and healthy breast tissues and molecular subtypes of breast cancer. *Front. Oncol.* **2016**, *6*, 126. [CrossRef] [PubMed]
43. Yoshikawa, M.I.; Ohsumi, S.; Sugata, S.; Kataoka, M.; Takashima, S.; Mochizuki, T.; Ikura, H.; Imai, Y. Relation between cancer cellularity and apparent diffusion coefficient values using diffusion-weighted magnetic resonance imaging in breast cancer. *Radiat. Med.* **2008**, *26*, 222–226. [CrossRef] [PubMed]